A THEORETICAL CRITICAL HEAT FLUX MODEL FOR ROD BUNDLES UNDER PRESSURIZED WATER REACTOR CONDITIONS

WEN-SHAN LIN and BAU-SHEI PEI *National Tsing-Hua University*
Department of Nuclear Engineering, Hsinchu, Taiwan 30043

CHIEN-HSIUNG LEE *Institute of Nuclear Energy Research*
Thermohydraulic Laboratory, P.O. Box 3-3, Lungtan, Taiwan 32500

I. A. MUDAWWAR *Purdue University*
Boiling and Two-Phase Flow Laboratory
School of Mechanical Engineering, West Lafayette, Indiana 47907

Received March 17, 1988
Accepted for Publication November 30, 1988

A theoretical critical heat flux (CHF) model based on microlayer dryout and Helmholtz instability for subcooled tube flow under pressurized water reactor operation conditions is first extended to the conditions of saturated low-quality flow. Then the applicability of this extended theoretical CHF model to rod bundles is evaluated. The effects of grid spacers, cold wall, and axial heat flux nonuniformity on bundle CHFs are investigated.

The extended CHF model is very accurate when compared with three other well-known CHF correlations on a data base of round tube CHF. In the simple case with uniform axial heat flux distribution, simple grid spacers, and no guide tubes in bundles, the theoretical CHF model gives good results. In other more complex cases, the cold-wall effects due to the existence of guide tubes, the effects of mixing vane grids, and the effects of nonuniform axial heat flux distributions on CHF are significant. The present model generally gives satisfactory results when compared with ~1400 bundle CHF experimental data points although corrections for grid spacers, cold wall, and axial heat flux have not yet been considered.

I. INTRODUCTION

Among the various heat transfer phenomena, critical heat flux (CHF) is perhaps the most important for the design and safe operation of nuclear power reactors. Many articles have been published during the last 30 years on the investigation of CHF, and many empirical correlations have been developed for the accurate prediction of CHF. However, there are few theoretical CHF models presented in the literature, especially for forced convective low-quality CHF (departure from nucleate boiling), which is the most common type of boiling crisis in pressurized water reactors (PWRs). Lee and Mudawwar[1] and Weisman and Pei[2] have presented two theoretical models that have been widely evaluated against experimental data under PWR conditions with good accuracy.

Other theoretical models have limited application to PWR design. For instance, the well-known Haramura and Katto model[3] applies only to saturated pool boiling and external flow boiling conditions under atmospheric pressure. Bergel'son's model[4] is limited to subcooled conditions under low or medium pressure; in addition, its validity is questionable because its data base includes only ~30 experimental data points. Smogalev's model[5] was developed for low-flow conditions only. Yagov and Puzin's model[6] can only be used when local equilibrium quality is negative. Chernobai's model[7] is based on the assumption of critical liquid enthalpy; however, this assumption does not have any experimental support. Hebel et al.'s model[8] was developed to determine lower conservative limits of heat flux density, and its applicable ranges were not reported in their paper. Serizawa's model[9] was developed for external flow under power transients only.

Weisman and Pei's model was successfully extended to predict CHF in rod bundles under PWR conditions by Weisman and Ying[10] and by Ying and Weisman.[11] Hence, extending the applicable range of

TABLE X

Effects of Cold Wall (Guide Tubes) on CPRs of the Present Model

Test Section	Number of Data Points	R_{av}	Standard Deviation	C_g	GS	Guide Tube
131	25	1.0016	0.0439	1.400	26.0	No
138	30	1.0702	0.0539	1.400	26.0	Yes
164	34	0.9660	0.0443	1.250	22.0	No
162	36	1.0726	0.0514	1.250	22.0	Yes

TABLE XI

Effects of Axial Heat Flux Nonuniformity on CPRs of the Present Model

Test Section	Number of Data Points	R_{av}	Standard Deviation	C_g	GS	Profile	Guide Tube
68	67	0.8881	0.0269	1.430	14.2	B	Yes
71	49	0.9042	0.0341	1.430	14.2	D	Yes
117	37	0.8374	0.0715	1.407	20.0	E	No
132	25	0.9144	0.0328	1.400	20.0	I	No

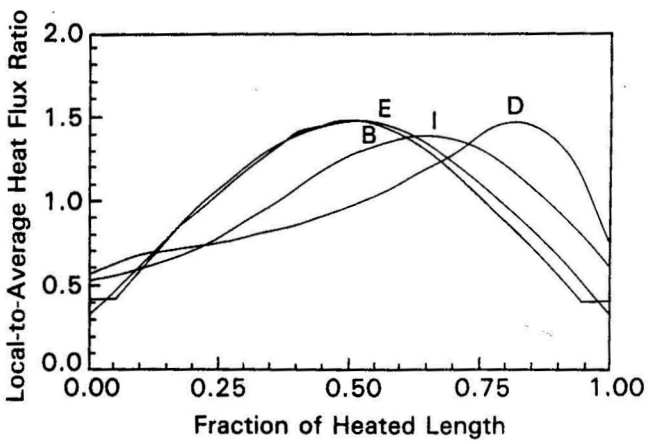

Fig. 4. Nonuniform axial heat flux distributions.[33]

As noted earlier, the value of the turbulent mixing parameter used in this research is 0.02, and it is not the real value for bundles with mixing vanes. Therefore, the effects of axial heat flux nonuniformity on CHF may be confounded with the effects of mixing vanes. Hence, the effects of heat flux nonuniformity should be investigated further in future studies after clearly defining the effects of mixing vanes.

V.B.7. Overall Assessment of Accuracy

In spite of the effects of grid spacers, cold walls, and heat flux nonuniformity discussed in the previous sections, it is worthwhile to assess the overall validity of the present model.

TABLE XII

Statistical Results of Bundle CHF Prediction with Uniform Axial Heat Flux Distribution

Correlation	Number of Data Points	R_{av}	rms	Standard Deviation
CHFR				
W-3	380	1.0345	0.2475	0.2451
EPRI-1	380	0.9873	0.0781	0.0771
Present model	377	1.0373	0.2175	0.2143
CPR				
W-3	250	0.9836	0.0922	0.0907
EPRI-1	243	0.9616	0.0894	0.0808
Present model	257	0.9776	0.0921	0.0894

Table XII shows the statistical results of CPRs based on the bundle CHF data with uniform axial heat flux distributions and no guide tubes. Table XIII shows the statistical results of CPRs based on the bundle CHF data with nonuniform axial heat flux distributions. The two well-known correlations, W-3 (Ref. 36) and EPRI-1 (Ref. 34), are also used for comparison.

TABLE XIII

Statistical Results of Bundle CHF Prediction with Nonuniform Axial Heat Flux Distributions

Correlation	Number of Data Points	R_{av}	rms	Standard Deviation
CHFR				
W-3	2346	0.9303	0.2934	0.2850
EPRI-1	2373	1.0189	0.1107	0.1090
Present model	2319	1.0223	0.2838	0.2829
CPR				
W-3	1160	0.9484	0.1040	0.0903
EPRI-1	1161	0.9822	0.0942	0.0925
Present model	1157	0.9589	0.1120	0.1042

The EPRI-1 correlation is one of the most accurate correlations for rod bundles under PWR conditions.[41] In addition, the applicable range of EPRI-1 is so wide that it covers nearly the whole range of practical applications. In the present comparison, the W-3 correlation for rod bundle CHF predictions has been corrected for grid spacers, cold wall, and axial heat flux nonuniformity, and the EPRI-1 correlation has been corrected for grid spacers and axial heat flux nonuniformity. As shown in Tables XII and XIII, the accuracy of the present theoretical CHF model is close to that of the W-3 and EPRI-1 correlations even though the present model has not corrected for these three effects. This is not surprising since these unconsidered effects may be partly compensated by one another under some circumstances. From the above evaluation, it is shown that the present model has a lot of potential in practical applications. It is believed that the present theoretical CHF model can also be refined further after adopting corrections for grid spacers, cold walls, and axial heat flux nonuniformity.

Figure 5 shows the parametric analysis of CPR on system pressure based on the present model for test points with nonuniform axial heat flux distributions. It can be seen from Fig. 5 that the majority of points falls in the ±20% range. However, it is also shown in Fig. 5 that the present theoretical CHF model loses its validity under system pressure of ~7 MPa or less.

VI. CONCLUSIONS AND FUTURE WORK

The following conclusions are drawn from the present investigation:

1. The present extended theoretical CHF model is very accurate for tube CHF of subcooled and saturated low-quality boiling flow.

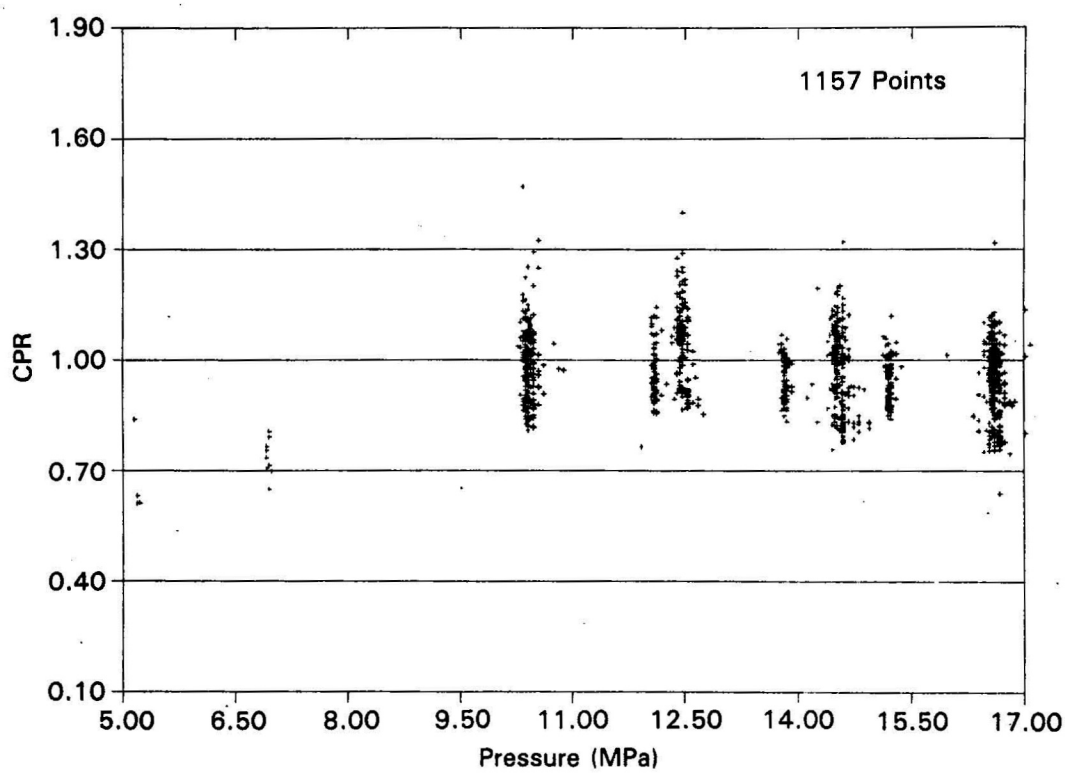

Fig. 5. Critical power ratio of the present model versus the system pressure.

2. The simplified numerical procedure for calculating the CPR is fairly accurate for comparing different models and correlations.

3. The present extended theoretical CHF model has been successfully applied to simple rod bundles of uniform axial heat flux, simple grid spacers, and no guide tubes under PWR conditions.

4. The effects of grid spacers, cold walls, and heat flux nonuniformity on CHF are significant and consistent with physical phenomena.

5. From an overall viewpoint, the present model has a lot of potential for practical application.

The following tasks should be accomplished in the near future:

1. The near-wall bubble behavior for high-heat flux boiling flow needs further investigation.

2. The thermodynamic nonequilibrium effects on CHFs for this extended theoretical CHF model must be studied further to make this model more realistic.

3. The model must be adjusted to account for the effects of grid spacers, cold wall, and axial heat flux nonuniformity on the CHF to improve the accuracy of bundle CHF predictions.

NOMENCLATURE

a_1 = 0.35, empirical constant

a_2 = 240, empirical constant

a_3 = −0.8, empirical constant

a_4 = 0.175, empirical constant

Bo = boiling number

C = parameter in Eq. (10)

C_0 = distribution parameter in drift-flux model

C_d = drag coefficient

C_g = loss coefficient of grid spacers

C_p = liquid specific heat under constant pressure

CP_m = measured critical power

CP_p = predicted critical power

D_b = vapor blanket diameter

D_w = tube diameter or subchannel wetted equivalent diameter

F_b = buoyancy force

F_d = drag force

F_I = inertial force due to vapor generation

F_R = lateral force due to circulation of vapor blanket

f = fanning friction factor for turbulent flow

G = local bulk mass flux

G_L = liquid mass flux

G_m = liquid mass flux flowing into microlayer

GS = axial spacing of grid spacers

g = gravitational acceleration

h_b = local bulk enthalpy

h_f = saturated liquid enthalpy

h_{fg} = latent heat

h_m = enthalpy of liquid flowing into microlayer

$h_{1\phi}$ = single-phase heat transfer coefficient

h_{sc} = heat transfer coefficient of subcooled boiling

K_f = conductivity of saturated liquid

L_m = length of vapor blanket

Pr = Prandtl number, $C_p\mu_f/K_f$

P_R = reduced pressure

q_c'' = predicted CHF

q_l'' = local heat flux

R_{av} = average value of CPR, CHFR, or R_{CPR}

R_{CPR} = ratio of approximated CPR to real CPR

Re = Reynolds number, GD_w/μ_f

Re_L = liquid Reynolds number

RPF = radial power peaking factor

T_b = bulk temperature

T_{sat} = saturation temperature

U_b = vapor blanket velocity

U_{bL} = liquid velocity at $y = \delta_m + D_b/2$

U_{gj} = drift velocity

U_L = liquid velocity

U_m = liquid velocity in the microlayer

U_t = friction velocity

X_e = bulk equilibrium quality

X_t = bulk true quality

y = distance from the wall

Z_{CHF} = location that CHF occurs

Greek

α = void fraction

β = turbulent mixing parameter

δ_m = microlayer thickness

ΔU = $U_b - U_{bL}$

μ = viscosity

ρ = density

σ = surface tension

τ_w = wall shear stress

Subscripts

b = bulk or bubble

f = saturated liquid

g = saturated vapor

fg = difference between saturated liquid and vapor

L = local or liquid

m = microlayer

ACKNOWLEDGMENTS

The authors are deeply indebted to Yi-Bin Chen, Chunkuan Shih, Lih-Yih Liao, Lainsu Kao, and Chin Pan for their helpful discussions and criticism.

The authors are obliged to the Institute of Nuclear Energy Research for its sponsorship of this research project.

REFERENCES

1. C. H. LEE and I. A. MUDAWWAR, "A Mechanistic Critical Heat Flux Model for Subcooled Flow Boiling Based on Local Bulk Flow Conditions," *Int. J. Multiphase Flow* (in press).

2. J. WEISMAN and B. S. PEI, "Prediction of Critical Heat Flux in Flow Boiling at Low Qualities," *Int. J. Heat Mass Transfer*, **26**, *10*, 1463 (1983).

3. Y. HARAMURA and Y. KATTO, "A New Hydrodynamic Model of Critical Heat Flux Applicable Widely to Both Pool and Forced Convection Boiling on Submerged Bodies in Saturated Liquids," *Int. J. Heat Mass Transfer*, **26**, *3*, 389 (1983).

4. B. R. BERGEL'SON, "Burnout Under Conditions of Subcooled Boiling and Forced Convection," *Thermal Eng.*, **27**, *1*, 48 (1980).

5. I. P. SMOGALEV, "Calculation of Critical Heat Fluxes with Flow of Subcooled Water at Low Velocity," *Thermal Eng.*, **28**, *4*, 208 (1981).

6. V. V. YAGOV and V. A. PUZIN, "Burnout Under Conditions of Forced Flow of Subcooled Liquid," *Thermal Eng.*, **32**, *10*, 569 (1985).

7. V. A. CHERNOBAI, "Model for Heat-Transfer Crisis for Water Boiling in Pipes," *High Temp.*, **18**, *5*, 797 (1980).

8. W. HEBEL, W. DETAVERNIER, and M. DECRETON, "A Contribution to the Hydrodynamics of Boiling Crisis in a Forced Flow of Water," *Nucl. Eng. Des.*, **64**, 433 (1981).

9. A. SERIZAWA, "Theoretical Prediction of Maximum Heat Flux in Power Transients," *Int. J. Heat Mass Transfer*, **26**, *6*, 921 (1983).

10. J. WEISMAN and S. H. YING, "A Theoretically Based Critical Heat Flux Prediction for Rod Bundles at PWR Conditions," *Nucl. Eng. Des.*, **85**, 239 (1985).

11. S. H. YING and J. WEISMAN, "Prediction of the Critical Heat Flux in Flow Boiling at Intermediate Qualities," *Int. J. Heat Mass Transfer*, **29**, *11*, 1639 (1986).

12. R. BOWRING and P. MORENO, "COBRA IIIC/MIT Computer Code Manual," Massachusetts Institute of Technology, Department of Nuclear Engineering (Mar. 1976).

13. R. MESLER, "A Mechanism Supported by Extensive Experimental Evidence to Explain High Heat Flux Observed During Nucleate Boiling," *AIChE J.*, **22**, 246 (1976).

14. A. M. BHAT, R. PRAKASH, and J. S. SAINI, "Heat Transfer in Nucleate Pool Boiling at High Heat Flux," *Int. J. Heat Mass Transfer*, **26**, 833 (1983).

15. R. HINO and T. UEDA, "Studies on Heat Transfer and Flow Characteristics in Subcooled Flow Boiling—Part 2, Flow Characteristics," *Int. J. Multiphase Flow*, **11**, 283 (1986).

16. S. B. V. MOLEN and F. W. B. M. GALJEE, "The Boiling Mechanism During Burnout Phenomena in Subcooled Two Phase Water Flow," *Proc. 6th Int. Heat Transfer Conf.*, Toronto, Canada, August 7–11, 1978, Vol. 1, p. 381.

17. M. M. SHAH, "A General Correlation for Heat Transfer During Subcooled Boiling in Pipes and Annuli," *ASHRAE Trans.*, **83**, *1*, 202 (1977).

18. R. COLE and W. R. ROHSENOW, "Correlation of Bubble Departure Diameters for Boiling of Saturated Liquids," *Chem. Eng. Progr. Symp.*, **92**, 211 (1969).

19. S. W. BEYERLEIN, R. K. COSSMANN, and H. J. RICHTER, "Prediction of Bubble Concentration Profiles in Vertical Turbulent Two-Phase Flow," *Int. J. Muiltiphase Flow*, **11**, *5*, 629 (1985).

20. B. K. C. CHAN and R. G. B. PRINCE, "Viscous Drag on a Gas Bubble Rise in a Liquid," *AIChE J.*, **11**, 188 (1965).

21. N. ZUBER and J. FINDLAY, "Average Volumetric Concentration in Two-Phase Flow Systems," *Trans. ASME, J. Heat Transfer*, **87**, 453 (1965).

22. J. G. COLLIER, *Convection Boiling and Condensation*, 2nd ed., p. 75, McGraw-Hill Book Company, Inc., London (1980).

23. R. A. DEBORTOLI, S. J. GREEN, B. W. LETOURNEAU, M. TROY, and A. WEISS, "Forced Convection Heat Transfer Burnout Studies for Water in Rectangular Channels and Round Tubes at Pressures Above 500 psia," WAPD-188, Bettis Atomic Power Laboratory (1958).

24. K. M. BECKER, P. PERSSON, L. NILSSON, and O. ERIKSSON, "Measurements of Burnout Conditions for Flow of Boiling Water in Vertical Round Ducts," Parts 1 and 2, AE-87 (1962) and AE-114 (1963), Aktiebolaget Atomenergie, Sweden.

25. D. H. LEE and J. D. OBERTELLI, "An Experimental Investigation of Forced Convection Burnout in High Pressure Water, Part 1. Round Tubes with Uniform Flux Distribution," UKAEA Rep. No. AEEW-R213, U.K. Atomic Energy Establishment, Winfrith (1963).

26. B. THOMPSON and R. V. MACBETH, "Boiling Water Heat Transfer Burnout in Uniformly Heated Round Tubes—A Compilation of World Data with Accurate Correlations," AEEW-R356, U.K. Atomic Energy Authority, Winfrith (1964).

27. D. H. LEE and D. J. MORRIS, "Burnout and Two-Phase Pressure Drop for Water at 1000 psia in Round Tubes with Uniform and Non-Uniform Heat Flux Distribution," AEEW-355, U.K. Atomic Energy Establishment, Winfrith (1964).

28. R. R. HOOD and L. ISAKOFF, "Heavy Water Moderated Power Reactors Progress Report for June 1962," USAEC D.P. 755, U.S. Atomic Energy Commission (1962).

29. R. J. WEATHERHEAD, "Nucleate Boiling Characteristics and the Critical Heat Flux Occurrence in Subcooled Axial Flow Water Systems," ANL-6675, Argonne National Laboratory (1963).

30. B. MATZNER, "Basic Experimental Studies of Boiling Fluid Flow and Heat Transfer at Elevated Pressures," TID-18978, U.S. Atomic Energy Commission (1962).

31. D. H. LEE and J. D. OBERTELLI, "An Experimental Investigation of Forced Convection Boiling in High Pressure Water," Part III, AEEW-R355, U.K. Atomic Energy Establishment, Winfrith (1965).

32. V. Y. DOROSHCHUK and F. P. FRIED, "Critical Heat Flux for Water Flowing in Tubes," *Problems of Heat Transfer and Hydraulics of Two-Phase Media*, Chap. 4, S. S. KUTADELADZE, Ed., Pergamon Press, Oxford (1969).

33. C. F. FIGHETTI and D. G. REDDY, "Parametric Study of CHF Data, Vol. 3: Critical Heat Flux Data," EPRI-NP-2609, Electric Power Research Institute (1983).

34. D. G. REDDY and C. F. FIGHETTI, "Parametric Study of CHF Data, Vol. 2: A Generalized Subchannel CHF Correlation for PWR and BWR Fuel Assemblies," EPRI-NP-2609, Electric Power Research Institute (1983).

35. M. E. NISSLEY, A. J. FRIEDLAND, and R. P. KNOTT, "Considerations for Comparing CHF Correlations," *Proc. 2nd Int. Topl. Mtg. Nuclear Power Plant Thermal Hydraulics and Operations*, Tokyo, Japan, April 15–17, 1986.

36. L. S. TONG, "Prediction of Departure from Nucleate Boiling for an Axially Non-Uniform Heat Flux Distribution," *J. Nucl. Energy*, **21**, 241 (1967).

37. R. W. BOWRING, "A Simple But Accurate Round Tube Uniform Heat Flux, Dryout Correlation over the Pressure Range 0.7–17 MN/m^2 (100–2500 psia)," AEEW-R789, U.K. Atomic Energy Establishment, Winfrith (1972).

38. Y. KATTO and H. OHNO, "An Improved Version of the Generalized Correlation of Critical Heat Flux for the Forced Convective Boiling in Uniformly Heated Vertical Tubes," *Int. J. Heat Mass Transfer*, **27**, *9*, 1641 (1984).

39. J. WEISMAN, J. C. LIM, and S. H. YING, "DNB Prediction in Assemblies with Mixing Vanes and Unheated Tubes," *Trans. Am. Nucl. Soc.*, **53**, 548 (1986).

40. L. S. TONG, "Boiling Crisis and Critical Heat Flux," TID-25887, AEC Critical Review Series, U.S. Atomic Energy Commission (1972).

41. B. S. PEI, Y. B. CHEN, C. SHIH, and W. S. LIN, "Evaluations and Modifications of the EPRI-1 Correlation on PWR Critical Heat Flux Predictions Under Normal and Abnormal Fuel Conditions," *Nucl. Technol.*, **75**, 134 (1986).

Lee and Mudawwar's theoretical CHF model to PWR rod bundles is important to basic research and also to practical applications. Following Weisman and Ying's contributions,[10,11] this becomes the second theoretical CHF model that can be applied to rod bundle geometries.

Since Lee and Mudawwar's theoretical CHF model is merely based on local bulk conditions, the subchannel analysis code COBRA IIIC/MIT-1 (Ref. 12) is used to predict the local subchannel average mass flux and the equilibrium quality in rod bundles.

II. THEORETICAL CHF MODEL

II.A. Review of the Theoretical CHF Model

Recently, Lee and Mudawwar presented a theoretical CHF model[1] under forced convection, subcooled boiling conditions. This model is based on microlayer dryout under a vapor blanket. Several articles[9,13-16] have proved the existence of the microlayer under high-heat flux, nucleate boiling conditions.

Theoretical models by Haramura and Katto[3] and Serizawa[9] are also based on microlayer dryout; however, these two models have very limited application, as noted in Sec. I.

Lee and Mudawwar[1] proposed the following assumptions for developing their theoretical CHF model:

1. Critical heat flux occurs as a result of local microlayer dryout after the onset of Helmholtz instability at the microlayer/vapor interface, as illustrated in Fig. 1.

2. The thickness of the liquid microlayer can be determined by a force balance on the vapor blanket in a direction normal to the wall, as illustrated in Fig. 2.

3. The formation of the vapor blanket results from the accumulation of bubbles as a vertical distorted vapor cylinder.

4. The equivalent diameter of the vapor blanket is assumed to be equal to the bubble departure diameter.

5. The length of the vapor blanket is assumed to be the same as the Helmholtz critical wavelength.

6. The velocity of the vapor blanket in the turbulent stream is assumed to be the superposition of the local liquid velocity and the relative velocity of the vapor blanket to the local liquid velocity. The relative velocity is assumed to be determined by a balance of buoyancy force and drag force acting on the vapor blanket.

Based on these assumptions, Lee and Mudawwar predicted the subcooled flow CHF using analytical formulations of the physical phenomena. Detailed derivations can be found in Ref. 1, and only a brief review is presented here.

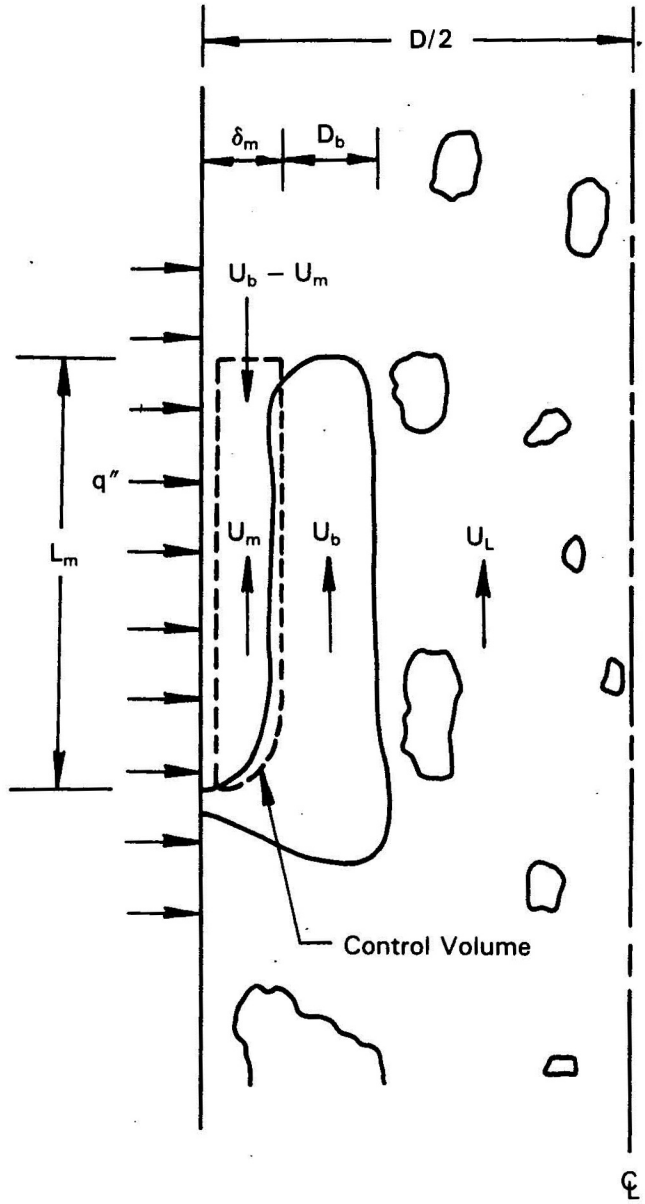

Fig. 1. Schematic illustrating the onset of microlayer dryout.[1]

Based on assumption 1, the CHF can be expressed by the following equation based on energy conservation of the microlayer[1] (see Nomenclature on p. 224):

$$q_c'' = G_m \delta_m [h_{fg} + (h_f - h_m)]/L_m$$
$$= G_m \delta_m [h_{fg} + a_1 (h_f - h_b)]/L_m \ , \quad \text{if } h_f > h_b \ , \tag{1}$$

where a_1 is an empirical constant.

The length of the vapor blanket L_m is assumed to be equal to the Helmholtz critical wavelength; i.e.,

$$L_m = 2\pi\sigma(\rho_f + \rho_g)/[\rho_f \rho_g (U_b - U_m)^2] \ . \tag{2}$$

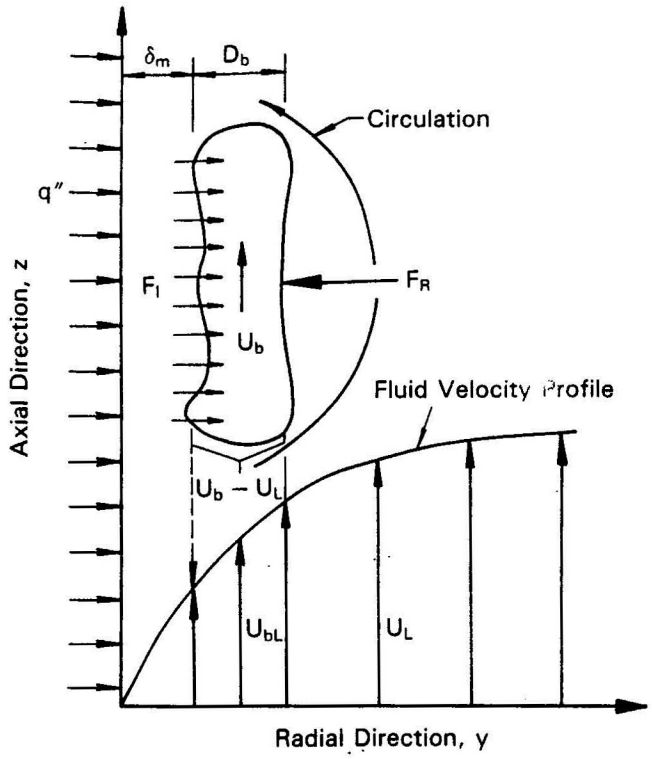

Fig. 2. Schematic of a vapor blanket moving in vertical flow before the onset of CHF (Ref. 1).

Since U_b is always much larger than U_m, the expression (2) can be reduced as follows:

$$L_m \simeq 2\pi\sigma(\rho_f + \rho_g)/(\rho_f \rho_g U_b^2) \ . \quad (3)$$

By definition, the liquid mass flux flowing into microlayer G_m is obtained as

$$G_m = \rho_f(U_b - U_m) \simeq \rho_f U_b \ . \quad (4)$$

Based on assumption 2, the inertial force (or the "momentum transfer rate into the vapor blanket" according to Ref. 1) due to vapor generation F_I is proposed to balance the force due to vapor blanket circulations F_R (Ref. 1). The thickness of liquid microlayer δ_m can then be determined. Hence, from the force balance,

$$F_I + F_R = 0 \ , \quad (5)$$

and F_I is derived[1] as follows:

$$F_I = \frac{[q_c'' - a_1 h_{sc}(T_{sat} - T_b)]^2 D_b L_m}{\rho_g h_{fg}^2} \ , \quad (6)$$

where h_{sc} is the subcooled boiling heat transfer coefficient that can be obtained by rearranging Shah's correlation[17] for high-heat flux boiling conditions, assuming that no heat transfer occurs between the blanket and the subcooled liquid in the core region. That is,

$$h_{sc} = \frac{230 q_c'' \, \mathrm{Bo}^{0.5}}{a_1(T_{sat} - T_b)(230\,\mathrm{Bo}^{0.5} - 1) + q_c''/h_{1\phi}} \ , \quad (7)$$

where Bo is the boiling number defined as $q_c''/(h_{fg}G)$ and $h_{1\phi}$ is the single-phase heat transfer coefficient, which is given by the well-known Dittus-Boelter equation,

$$h_{1\phi} = 0.023(K_f/D_w)\mathrm{Re}^{0.8}\mathrm{Pr}^{0.4} \ . \quad (8)$$

It is recommended that the diameter of the blanket D_b be obtained by Cole and Rohsenow's correlation[18]:

$$D_b = 1.5 \times 10^{-4}[\sigma/g(\rho_f - \rho_g)]^{1/2} \times (\rho_f C_p T_{sat}/\rho_g h_{fg})^{1.25} \ . \quad (9)$$

The lateral force due to vapor blanket circulation F_R can be expressed as

$$F_R = -C\rho_f(U_b - U_{bL})(\partial U_L/\partial y)\left(\frac{\pi}{4} D_b^2 L_m\right) \ . \quad (10)$$

The parameter C in Eq. (10) is a function of the liquid Reynolds number and the void fraction, as noted in Ref. 19. Hence, under subcooled flow boiling conditions, Lee and Mudawwar[1] suggested that C can be expressed by

$$C = a_2 \mathrm{Re}^{a_3} \ , \quad (11)$$

where a_2 and a_3 are empirical constants.

The liquid velocity at $y = \delta_m + D_b/2$ is calculated by the velocity profile in the buffer region of the three-layer velocity distribution. Hence,

$$U_{bL} = U_t\left\{5 \ln\left[\rho_f\left(\delta_m + \frac{D_b}{2}\right)U_t \Big/ \mu_f\right] - 3.05\right\} \ , \quad (12)$$

where U_t is the friction velocity defined as

$$U_t = (\tau_w/\rho_f)^{1/2} \ . \quad (13)$$

The wall shear stress τ_w can be obtained as

$$\tau_w = \frac{1}{2} f G^2/\rho_f = \frac{1}{2}(0.046\,\mathrm{Re}^{-0.2})G^2/\rho_f \ . \quad (14)$$

Similarly, the velocity gradient in Eq. (10) is[1]

$$\partial U_L/\partial y = 2.5 U_t\left(1 + \frac{\delta_m}{D_b + \delta_m}\right)\Big/\delta_m \ . \quad (15)$$

Following assumption 6, the vapor blanket velocity U_b is obtained by equating the buoyancy force F_b with the drag force F_d. Hence,

$$F_b + F_d = 0 \ ; \quad (16)$$

F_b and F_d can be expressed as

$$F_b = \frac{1}{4}\pi D_b^2 L_m g(\rho_f - \rho_g) \quad (17)$$

and

$$F_d = -\frac{1}{2}\rho_f C_d (U_b - U_{bL})^2 \frac{1}{4}\pi D_b^2 , \quad (18)$$

where C_d is the drag coefficient, which can be calculated by the correlation proposed by Chan and Prince[20] as

$$C_d = 48\mu_f/[\rho_f D_b (U_b - U_{bL})] . \quad (19)$$

By combining Eq. (1) and Eqs. (3) through (19), one can obtain the predicted CHF q_c'' by iterative calculations if the values of empirical constants a_1, a_2, and a_3 are known. The values of a_1, a_2, and a_3 were determined to be 0.35, 240, and −0.8, respectively, by Lee and Mudawwar.[1] Comparisons of model predictions with experimental tube CHF data of water show that this model is very successful in simulating the subcooled CHF.

II.B. Extension of the Theoretical CHF Model to Low-Quality Saturated Boiling Flow

In Eq. (11), the void fraction effects on parameter C are neglected for subcooled conditions. Under saturated, low-quality flow boiling conditions, these effects may become important and, therefore, should be taken into consideration. The parameter C is expressed by

$$C = a_2 \mathrm{Re}_L^{[a_3 - a_4\alpha/(1-\alpha)]} , \quad (20)$$

where Re_L is the liquid Reynolds number defined as

$$\mathrm{Re}_L = G_L D_w/\mu_f , \quad (21)$$

and the liquid mass flux G_L is defined as

$$G_L = G(1 - X_t)/(1 - \alpha) . \quad (22)$$

The empirical constants a_2 and a_3 in Eq. (20) are set at the original values given in Sec. II.A, and a_4 is empirically determined to have a value of 0.175. Note that Eq. (20) can be reduced to Eq. (11) when $\alpha = 0$.

Under the approximation of bulk thermodynamic equilibrium, the bulk true quality X_t can be obtained as follows:

$$\begin{cases} X_t \simeq 0 , & \text{if } h_b \le h_f ; \\ X_t \simeq X_e = (h_b - h_f)/h_{fg} , & \text{if } h_b > h_f . \end{cases} \quad (23)$$

Hence, the true quality can be obtained from the local bulk enthalpy, and the void fraction α can be calculated by using Zuber and Findlay's drift-flux model[21]:

$$\alpha = \frac{X_t}{C_0[X_t + (1 - X_t)\rho_g/\rho_f] + \rho_g U_{gj}/G} , \quad (24)$$

where the drift velocity U_{gj} and the distribution parameter C_0 can be calculated from the following equations[22]:

$$U_{gj} = 1.41[\sigma g(\rho_f - \rho_g)/\rho_f^2]^{1/4} \quad (25)$$

and

$$\begin{cases} C_0 = 1.2 , & \text{if } P_R \le 0.5 ; \\ C_0 = 1.2 - 0.4(P_R - 0.5) , & \text{if } P_R > 0.5 . \end{cases} \quad (26)$$

Equation (23) cannot accurately predict the true quality because the subcooled or low-quality boiling flow is generally under thermodynamic nonequilibrium conditions. This thermodynamic nonequilibrium effect on the present model should be studied further in the near future.

The wall shear stress τ_w is obtained by Eq. (14) when the mass flux G is replaced by the liquid mass flux G_L; i.e.,

$$\tau_w = \frac{1}{2}(0.046\,\mathrm{Re}_L^{-0.2})G_L^2/\rho_f . \quad (27)$$

By assuming that $h_m = h_f$ and $T_b = T_{sat}$ under saturated conditions, the energy conservation equation [Eq. (1)] and the expression of inertial force [Eq. (6)] must be revised as follows:

$$\begin{cases} q_c'' = G_m \delta_m h_{fg}/L_m , & \text{if } h_f \le h_b ; \\ q_c'' = G_m \delta_m [h_{fg} + a_1(h_f - h_b)]/L_m , & \text{if } h_f > h_b \end{cases} \quad (28)$$

and

$$\begin{cases} F_I = q_c''^2 D_b L_m/(\rho_g h_{fg}^2) , \\ \qquad\qquad \text{if } h_f \le h_b ; \\ F_I = [q_c'' - a_1 h_{sc}(T_{sat} - T_b)]^2 D_b L_m/(\rho_g h_{fg}^2) , \\ \qquad\qquad \text{if } h_f > h_b . \end{cases} \quad (29)$$

Using Eqs. (20) through (29), the model presented in Sec. II.A can be extended to predict CHF under low-quality saturated conditions. This extended low-quality flow CHF model is shown in Sec. V to be very accurate for vertical tube CHF. The applicable ranges of this extended CHF model are summarized in Table I. It can be seen from Table I that this theoretical CHF model can be applied over ranges that are wide enough for practical application under PWR conditions.

TABLE I

Applicable Ranges of the Present Extended CHF Model

Pressure (MPa)	4.9 to 17.6
Mass flux ($kg \cdot s^{-1}/m^2$)	1000 to 5000
Tube diameter (m)	0.004 to 0.016
Subcooling (K)	<50
Void fraction	<0.5

II.C. Calculation Procedure for the Present CHF Model

Since the model presented in Secs. II.A and II.B is very complicated, an efficient calculation procedure should be helpful to the user.

Before we present the calculation procedure, it is necessary to modify the expression for the vapor blanket velocity U_b. By combining Eqs. (3) and (16) through (19), the following equation can easily be derived:

$$U_b^3 - U_b^2 U_{bL} - [\pi\sigma g D_b(\rho_f^2 - \rho_g^2)/(12\mu_f\rho_f\rho_g)] = 0 \ . \tag{30}$$

Equation (30) always has only one real root that can be explicitly expressed as

$$U_b = S_1 + S_2 + \frac{U_{bL}}{3} \ , \tag{31}$$

where

$$S_1 = \left[\frac{S_3}{2} + \frac{U_{bL}^3}{27} + \left(\frac{S_3^2}{4} + \frac{S_3 U_{bL}^3}{27}\right)^{1/2}\right]^{1/3} ,$$

$$S_2 = \left[\frac{S_3}{2} + \frac{U_{bL}^3}{27} - \left(\frac{S_3^2}{4} + \frac{S_3 U_{bL}^3}{27}\right)^{1/2}\right]^{1/3} ,$$

and

$$S_3 = \pi\sigma g D_b(\rho_f^2 - \rho_g^2)/(12\mu_f\rho_f\rho_g) \ .$$

Hence, U_b is a function of U_{bL}, D_b, and fluid properties.

The calculation procedure is as follows:

1. Calculate X_t by Eq. (23), α by Eq. (24), G_L by Eq. (22), Re_L by Eq. (21), and D_b by Eq. (9).

2. Calculate τ_w by Eq. (27) and U_t by Eq. (13).

3. Estimate the microlayer thickness δ_m.

4. Calculate parameter C by Eq. (20), $\partial U_L/\partial y$ by Eq. (15), and U_{bL} by Eq. (12).

5. Calculate U_b by Eq. (31).

6. Calculate L_m by Eq. (3) and G_m by Eq. (4).

7. Calculate q_c'' by Eq. (28), h_{sc} by Eq. (7), and F_I by Eq. (29).

8. Combining Eqs. (5) and (10), $U_b - U_{bL}$ can be calculated as

$$\Delta U = U_b - U_{bL} = \frac{F_I}{C\rho_f(\partial U_L/\partial y)\left(\frac{\pi}{4} D_b^2 L_m\right)} \ . \tag{32}$$

9. Using the value of U_b calculated in step 5 and the value of ΔU obtained in step 8, a new value of U_{bL} is obtained:

$$U_{bL} = U_b - \Delta U \ . \tag{33}$$

If the value of U_{bL} obtained here is negative, it means that the δ_m estimated in step 3 is too large and a smaller value must be used to continue the iteration.

10. By rearranging Eq. (12) and using the new value of U_{bL} obtained in step 9, a new value of microlayer thickness δ_m can be obtained:

$$\delta_m = \left(\frac{\mu_f}{\rho_f U_t}\right)\exp\left[\left(\frac{U_{bL}}{U_t} + 3.05\right)\Big/5\right] - \frac{1}{2} D_b \ . \tag{34}$$

11. If the value of δ_m obtained in step 10 and that estimated in step 3 are not close enough, return to step 3. Otherwise, the value of q_c'' calculated in step 7 is the predicted CHF.

III. DATA BASE

A total of 679 round tube water CHF data points are collected from several different sources[23-32] to form a data base for the present model. These data points all fall in the applicable ranges of the present theoretical CHF model.

The data base of rod bundle CHF consists of the experimental data selected from the Heat Transfer Research Facility data bank at Columbia University.[33] About 1400 data points are selected from 44 test sections of typical PWR bundle geometries. Twenty-one test sections have uniform axial heat flux distributions, and the rest have nonuniform axial heat flux distributions. Since the peripheral and corner CHF events are atypical cases of fuel rod arrays in a PWR core, these events are not included in the data base. The parametric ranges covered by the data base of bundle CHF are shown in Table II.

TABLE II

Ranges Covered by the Bundle CHF Data Base

Reactor type	PWR
Bundle arrangement	3 × 3, 4 × 4, 5 × 5 square array
Heated length (m)	1.22 to 4.27
Rod diameter (m)	0.0095 to 0.0127
Axial heat flux distribution	Uniform and nonuniform
Radial peaking factor	1.000 to 1.211
System pressure (MPa)	5 to 17
Local equilibrium quality	−0.25 to 0.22
Local mass flux ($kg \cdot s^{-1}/m^2$)	1000 to 5000
Subchannel hydraulic diameter (m)	0.0117 to 0.0153
Bundle average heat flux (MW/m^2)	0.6 to 2.6

IV. COBRA IIIC/MIT-1 AND ITS INPUT OPTIONS

For the improved numerical scheme, the core subchannel thermal-hydraulic analysis code COBRA IIIC/MIT-1 used in this study is a faster running version of the COBRA IIIC code without loss of accuracy. COBRA IIIC is a standard thermal-hydraulic subchannel analysis code that is widely used in the nuclear industry. The role of the COBRA IIIC/MIT-1 code in the present study is to provide correct local subchannel average conditions for the present model or for other CHF correlations. This study is based on the input options suggested by Reddy and Fighetti[34] for running COBRA IIIC/MIT-1, as summarized in Table III. Note that the value of turbulent mixing parameter in Table III is 0.02. This may not be a realistic value for bundles with mixing vanes. However, in the absence of an accurate value for turbulent mixing parameter in the open literature, the authors rely on a sensitivity study in Sec. V to investigate the effects of this parameter on the predicted critical power.

V. COMPARISONS WITH CHF DATA

Predictions of the present theoretical CHF model are compared with experimental CHF data by examining the statistical results of critical power ratios (CPRs). The statistical results of critical heat flux ratios (CHFRs) are also examined for reference. The CPR is defined as

$$\text{CPR} = CP_p/CP_m \ , \tag{35}$$

where

CP_p = predicted critical power

CP_m = measured critical power.

The CHFR is defined as

$$\text{CHFR} = q_c''(CP_m, Z_{\text{CHF}})/q_l''(CP_m, Z_{\text{CHF}}) \ , \tag{36}$$

where

$q_c''(CP_m, Z_{\text{CHF}})$ = CHF predicted by the correlation at Z_{CHF} based on the local conditions calculated at measured critical power

$q_l''(CP_m, Z_{\text{CHF}})$ = local heat flux at Z_{CHF} under measured critical power

= measured CHF

Z_{CHF} = measured location where boiling crisis occurred.

A perfect CHF correlation gives the CPR and CHFR values of 1 for every test point. Hence, a statistical analysis of CPRs and CHFRs for the data set may indicate the accuracy of the correlation. However, as indicated by Nissley et al.,[35] the statistical analysis based on CPRs is more meaningful than on CHFRs for comparing the accuracy of CHF correlations. This is the reason why CPR is chosen as an indicator for the validity of correlations in this study.

TABLE III

Major Input Options of COBRA IIIC/MIT-1 in the Present Analysis

Parameter	Value or Correlation
Subcooled void fraction	Levy's correlation
Bulk void fraction	Homogeneous model
Two-phase friction multiplier	Homogeneous model
Turbulent mixing parameter	0.02
Single-phase friction factor	$f = 0.046\,\text{Re}^{-0.2}$
Turbulent momentum factor	0
Cross-flow resistance factor	0.5
Cross-flow momentum factor	0.5
Axial nodes	50
Convergence error	10^{-3}

V.A. Tube CHF Predictions

Table IV gives a summary of the statistical results based on the round tube experimental CHF data. The

TABLE IV

Statistical Results of CPRs of Round Tube CHF

Correlation	R_{av}	Root-Mean-Square (rms)	Standard Deviation
A. Subcooled Conditions (Data points = 235)			
W-3	1.0201	0.1240	0.1227
Bowring	0.9889	0.0729	0.0722
Katto and Ohno	0.9251	0.1296	0.1060
Present model	0.9937	0.0889	0.0889
B. Saturated Low-Quality Conditions (Data points = 444)			
W-3	0.9784	0.0734	0.0703
Bowring	0.9920	0.0764	0.0761
Katto and Ohno	0.9693	0.0945	0.0895
Present model	0.9962	0.0710	0.0710
C. Overall Results (Data points = 679)			
W-3	0.9928	0.0940	0.0939
Bowring	0.9909	0.0752	0.0747
Katto and Ohno	0.9540	0.1080	0.0978
Present model	0.9953	0.0777	0.0776

statistical results of three well-known CHF correlations, W-3 (Ref. 36), Bowring,[37] and Katto and Ohno,[38] are also shown for comparison. As shown in Table IV.A, Bowring's correlation is the most accurate among these correlations under subcooled conditions. In Table IV.B, it is shown that the present model is better than the others under saturated low-quality conditions. Table IV.C shows the statistical results of all tube CHF data points including both subcooled and saturated low-quality conditions; Bowring's correlation is the most accurate overall. However, the accuracy of the present CHF model is very close to that of Bowring's correlation. The next target of this research will be to assess the applicability of the present theoretical CHF model to rod bundles.

V.B. Bundle CHF Predictions

V.B.1. A Simplified Procedure to Calculate CPRs

For the calculation of CPRs in rod bundles, the predicted critical power can only be obtained by trial and error iterations from subchannel analysis with different bundle powers. This means that the CPR for every test point would require several runs of the COBRA IIIC/MIT-1 code. To save computer time, the simplified procedure used by Reddy and Fighetti[34] has been adopted in the present study. This procedure is based on two assumptions:

1. The local mass flux distribution computed by the COBRA IIIC/MIT-1 code remains unchanged at different power levels.
2. The enthalpy rise in subchannels is proportional to the bundle power.

In the region close to the measured critical power, this simplified procedure is believed to be accurate enough for the purpose of the present comparative study. Weisman and Ying[10] developed a similar procedure for saving computer time; however, the validity of this simplified procedure and that adopted by Weisman and Ying has not been examined rigorously. For this reason, the ratio R_{CPR} is defined in this study as

$$R_{CPR} = \text{approximated CPR/real CPR} , \quad (37)$$

where the real CPR is the CPR obtained without using the simplified procedure, and the approximated CPR is the CPR obtained by using the simplified procedure. If the simplified procedure is valid, the value of R_{CPR} for every data point will attain a value very close to unity. It follows that the statistical analysis of R_{CPR} will be an effective method for examining the validity of this simplified procedure in CPR predictions.

Table V shows the statistical results of R_{CPR}. The data points used in Table V are chosen at random from 11 test sections, all with a uniform axial heat flux distribution. The results of W-3 (Ref. 36) and EPRI-1 (Ref. 34) correlations are also presented for comparison. It can be seen from Table V that this simiplified procedure seems to be very accurate from the overall viewpoint for W-3, EPRI-1, and the present theoretical CHF model.

TABLE V

Statistical Results of R_{CPR}

(Approximated CPR/real CPR)

(Data points = 113)

Correlation	R_{av}	rms	Standard Deviation
W-3	1.0017	0.0036	0.0032
EPRI-1	1.0011	0.0030	0.0028
Present model	1.0016	0.0036	0.0033

Figure 3 shows the variation of R_{CPR} with quality for the present model. It seems that the simplified procedure gradually loses its validity as local equilibrium quality decreases. Similar trends also exist for W-3 and EPRI-1 correlations. Fortunately, the deviation from the true value is within the range of ±2%, as shown in Fig. 3. Hence, the simplified procedure is accurate enough for comparison. The analyses performed hereafter in this study are all based on the approximated CPRs to save computer time while maintaining sound accuracy.

V.B.2. Bundle CHF Predictions Under Conditions of Uniform Axial Heat Flux, Simple Grid Spacers, and No Guide Tubes

In the simple case of uniform axial heat flux, simple grid spacers, and no guide tubes in the bundles, it

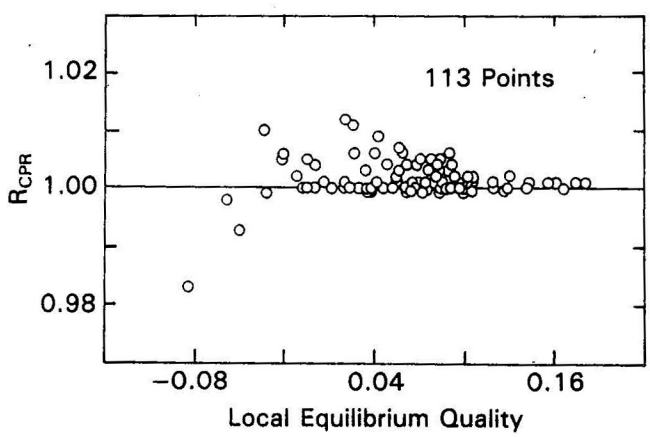

Fig. 3. R_{CPR} of the present model versus local equilibrium quality.

TABLE VI

Statistical Results of CPRs of the Present Model for Five Simple Test Sections

Test Section	PWR Vendor	Number of Data Points	R_{av}	Standard Deviation	C_g	GS
13	CE	18	1.0468	0.0333	0.815	16.0
14	CE	21	1.1041	0.0312	0.815	16.0
48	CE	23	1.0100	0.0399	0.815	14.3
201	EX	8	0.9928	0.1504	0.635	15.5
512	UN	27	0.9727	0.0524	0.570	10.0

is expected that the present model will give good agreement with the experimental results. Five test sections that belong to this simple case are chosen to explore the applicability of the present model at the first stage. As shown in Table VI, the present model seems to give good results, except for a slight overprediction to the Combustion Engineering (C-E) bundles.

Note that the results of test section 201 have a large standard deviation value although the value of R_{av} is close to unity. Similar results (not presented here) are also obtained by the W-3 and EPRI-1 correlations for the same test section. The reasons for these results are still under investigation.

V.B.3. Sensitivity Studies on the Turbulent Mixing Parameter

Under the conditions of uniform axial heat flux and no guide tubes in the bundles, the effects of mixing vanes on CHF are explored. As shown in Table VII, test sections 62, 136, 401, 407, and 405 have mixing vanes due to their lower R_{av} values. The mixing vanes in test bundles are expected to promote turbulent mixing and enhance the experimental CHF. As a result, the CPRs are expected to be lower than unity to some extent. The results of test sections 401, 407, and 405, in Table VII, show that the effects of mixing vanes seem to follow a well-defined trend with the radial power peaking factor *RPF*. That is, for the same type of mixing vanes, the R_{av} value decreases as *RPF* increases.

The results mentioned above are based on the turbulent mixing parameter of 0.02 since the real value of the turbulent mixing parameter for the mixing vanes is not available in the open literature. This value of 0.02 is considered to be smaller than the real value for mixing vanes. Weisman et al.[39] have claimed that the effects of mixing vanes can be well simulated by appropriately increasing the mixing parameter. Therefore, in the present study, three test points (A, B, and C) are sampled to explore the sensitivity of CHF predictions to the turbulent mixing parameter β. Point A is the data from test section 62 series 8; point B is the data from test section 136 series 27, and point C is the data from test section 405 series 16. As shown in Table VIII, the values of CPR for point A vary from 0.8827 to 0.9424 as the values of β vary from 0.02 to 0.10. Similarly, CPRs of points B and C vary from 0.8333 to 0.8992 and 0.8517 to 0.8799, respectively, in response to a fivefold increase in β. This range of β is believed to cover the real values of β for mixing vanes. Hence, as shown in Table VIII, using the correct value of β improves the CHF predictions to some extent, but the effects of mixing vanes on CHF cannot be simulated completely by only using the real β. The local

TABLE VII

Effects of Grid Spacers on CPRs of the Present Model Under the Conditions of Uniform Axial Heat Flux and No Guide Tubes

Test Section	Number of Data Points	R_{av}	Standard Deviation	C_g	GS	RPF
62	25	0.8974	0.0440	1.255	14.3	1.211
136	18	0.8379	0.0328	1.093	18.85	1.136
401	14	0.9887	0.0304	0.70	15.0	1.008
407	21	0.9314	0.0404	0.70	15.0	1.067
405	10	0.8627	0.0355	0.70	15.0	1.196

TABLE VIII

Effects of Turbulent Mixing Parameter on CPRs for the Present Model

Test Point	β						
	0.02	0.03	0.04	0.05	0.06	0.07	0.10
A	0.8827	0.9022	0.9149	0.9233	0.9295	0.9340	0.9424
B	0.8333	0.8481	0.8611	0.8718	0.8792	0.8860	0.8992
C	0.8517	0.8617	0.8678	0.8716	0.8743	0.8763	0.8799

velocity profiles, void fraction distributions, etc., within the subchannel are also influenced by mixing vanes, and these local parameters are important in defining the onset of CHF. However, the predictions of these local parameters are beyond the capability of the present subchannel analysis code COBRA IIIC/MIT-1.

V.B.4. Effects of Axial Spacing of Grid Spacers

The effects of axial spacing of grid spacers on CHF for the present theoretical CHF model are presented in Table IX, which shows test sections that have larger average values of CPR always correspond to larger axial spacing of grid spacers. These results can be explained by the mixing effects induced by grid spacers. The larger axial spacing of grid spacers induces less mixing, which in turn produces a smaller measured critical power and a larger CPR value.

V.B.5. Cold-Wall Effects

The effects of a cold (or unheated) wall on CHF are shown in Table X. It is well known that the guide tubes in a PWR rod bundle may induce the cold-wall effects since they cannot generate any thermal energy. Tong[40] noted that the existence of a cold wall reduces the cooling capability of the subchannel flow since the coolant near the cold wall cannot be used to cool the heating surface. Hence, a larger CPR value will be ended if the cold wall exists nearby. The results in Table X are consistent with Tong's observation.

V.B.6. Effects of Axial Heat Flux Nonuniformity

Table XI shows the effects of axial heat flux nonuniformity on the CHF. The axial heat flux profiles shown in Table XI are depicted in Fig. 4. As shown in Table XI, the test sections with profiles more skewed toward the outlet generally seem to have a larger average CPR value. This can be explained by the vapor accumulation effects near the critical point. As the heat flux profile becomes more skewed toward the test section outlet, more vapor is generated and accumulated near the critical point because the generated vapor has not had enough time to condense or diffuse into the bulk flow. As a result, more serious "wall conditions" are formed and the experimental CHF value decreases. This mechanism tends to drive the CPR to a larger value even though the correct "subchannel average conditions" are calculated by COBRA IIIC/MIT-1 when the real value of the turbulent mixing parameter is used.

TABLE IX

Effects of Axial Spacing of Grid Spacers on CPRs of the Present Model

Test Section	Number of Data Points	R_{av}	Standard Deviation	C_g	GS	Guide Tube
121	37	0.8407	0.0796	1.200	20.0	No
124	32	0.8348	0.0645	1.200	20.0	No
114	33	0.9465	0.0640	1.200	26.0	No
125	33	0.8319	0.0581	0.680	20.0	No
127	37	0.8681	0.0459	0.680	22.0	No
133	22	0.9001	0.0165	1.400	13.0	No
132	25	0.9144	0.0328	1.400	20.0	No
131	25	1.0016	0.0439	1.400	26.0	No
134	24	1.0410	0.0459	1.400	32.0	No